J Mater Sci (2013) 48:4524–4532
DOI 10.1007/s10853-012-6979-9

NANOSTRUCTURED MATERIALS

Three-dimensional analysis of plastic flow during high-pressure torsion

Roberto B. Figueiredo · Gustavo C. V. de Faria · Paulo R. Cetlin · Terence G. Langdon

Received: 3 September 2012 / Accepted: 18 October 2012 / Published online: 9 November 2012

Abstract The use of imposed plastic deformation as a single parameter to compare results of samples processed by severe plastic deformation is not always accurate. Therefore, this report describes the theoretical plastic flow occurring during high-pressure torsion and presents finite element modeling of this technique to complement the theory. The results demonstrate the influence on plastic flow of the material behavior, the sample aspect ratio, the processing pressure, and the contact friction between the sample and the anvil. It is shown that heterogeneous flow is primarily observed near the edges of the samples. The present results are in general agreement with published experimental observations.

Introduction

Severe plastic deformation (SPD) techniques [1] are now widely used to process metallic materials in order to refine the grain structure to the submicron level and to promote changes in their mechanical properties. Among the different SPD techniques, the most commonly used are equal-channel angular pressing (ECAP) [2] and high-pressure torsion (HPT) [3]. The former is simpler and can be easily adapted to a conventional pressing machine but the latter is more effective in achieving grain refinement and may be used relatively easily to process difficult-to-work materials. For both procedures, the characteristics of the processing operation and the results obtained are dependent upon the equipment used and the specific die or anvil geometry. Thus, in order to compare the experimental results for materials processed using different facilities, it is necessary to develop a detailed understanding of the role of each processing parameter on the material flow.

In general, the basic approach in SPD processing consists of determining the influence of a selected processing parameter on the theoretical distribution of plastic deformation imposed to the sample and then using this parameter to provide a unique characterization of the processing operation. An example is processing by ECAP where the theoretical distribution of plastic strain has been determined as a function of the angle between the channels and the outer arc of curvature at the point of intersection between the two channels in the die [4]. Many reports make use of this single parameter to compare the results obtained for structural characterization and mechanical testing for samples processed using different ECAP facilities and dies. In general, the correlation is reasonably satisfactory but it is now well established that there are also minor variations in the structural evolution and mechanical properties for materials processed to similar levels of plastic strain using different die angles [5], different processing routes [6], and different processing temperatures [7]. Moreover, variations have been reported in the

R. B. Figueiredo (✉)
Department of Materials Engineering and Civil Construction, Universidade Federal de Minas Gerais, Belo Horizonte, MG 31270-901, Brazil
e-mail: figueiredo-rb@ufmg.br

G. C. V. de Faria · P. R. Cetlin
Department of Mechanical Engineering, Universidade Federal de Minas Gerais, Belo Horizonte, MG 31270-901, Brazil

T. G. Langdon
Materials Research Group, Faculty of Engineering and the Environment University of Southampton, Southampton SO17 1BJ, UK

T. G. Langdon
Departments of Aerospace & Mechanical Engineering and Materials Science, University of Southern California, Los Angeles, CA 90089-1453, USA

distributions of microhardness along longitudinal sections of samples processed by ECAP [8, 9]. It follows, therefore, that comprehensive analyses are needed, using a procedure such as finite element modeling (FEM), to obtain a more detailed understanding of the nature of the plastic flow and specifically the influence of a range of processing parameters.

Several reports have been published describing the use of FEM in modeling the flow behavior in ECAP and incorporating the effect of diverse processing parameters on the distribution of strain, stress and damage [10–13]. These various analyses are usually compared to experimental results and they provide an increased understanding of the flow processes. By contrast, very little information is currently available on the flow processes occurring in HPT. The present investigation was initiated to provide a more complete understanding of flow processes in HPT with an emphasis on the initial sample thickness, the evolution of flow stress with strain, the applied pressure, and frictional effects. The following section provides a detailed description of HPT processing and the next section outlines the results obtained using FEM.

The principles of HPT

A theoretical description of HPT

The basic principles of the HPT processing technique are illustrated in Fig. 1. A sample, in the form of a thin disk, is placed between massive rigid anvils so that it is contained within depressions on the upper and lower surfaces of the two anvils. A compressive force is applied between the anvils leading to a compressive stress state and then one of the anvils is rotated to introduce torsional straining to the disk. In practice, the surface roughness in the depressions of the two anvils increases the contact friction between the disk and the anvils thereby preventing slippage and leading to a true torsional deformation of the sample.

A basic approach in HPT is to obtain experimental results, such as microhardness measurements, and then to determine the theoretical amount of plastic deformation imposed on the sample. In this way, it is feasible to make direct comparisons between experimental results obtained at similar levels of deformation. The theoretical value of the effective strain, ε, imposed in torsion is given by the relationship [14]:

$$\varepsilon = \frac{2\pi Nr}{h\sqrt{3}}, \quad (1)$$

where N is the number of complete turns in HPT, r is the distance from the center of rotation, and h is the sample height (or thickness). It follows from Eq. 1 that there is a linear relationship between the radial distance and the amount of strain so that the anticipated theoretical distribution of strain in the disk surface is illustrated in Fig. 2a. This strain varies from zero at the disk center and increases linearly in all directions toward a maximum value at the edge of the disk.

Metallic materials usually exhibit strain-hardening behavior when deformed at low homologous temperatures so that processing by HPT is expected to increase the material strength. The generally accepted relationship between stress and strain is where the flow stress, σ, is proportional to ε^n, where ε is the strain and n is the strain-hardening exponent. Using this relationship, the flow stress is expected to exhibit the distribution shown in Fig. 2b. Thus, a finite value of flow stress is expected near the center of the sample, there is a pronounced increase in stress at reduced distances from the center and thereafter there is a gradual saturation in the stress at larger distances. Considering the flow stress as a reasonable measure of the material strength, it is anticipated that the sample will exhibit a heterogeneous variation in strength across the disk surface.

The hydrostatic stress is usually calculated as the compressive force divided by the area of the sample. In practice, it is considered as a constant throughout the sample and it has no theoretical influence on the distribution of plastic deformation.

Experimental observations and the significance of using FEM

Numerous reports have shown that samples processed by HPT exhibit increasing hardness with increasing distance from the center of the disk after low numbers of rotations [15–21]. However, at higher numbers of turns, the hardness in the central region of the disk increases and there is a corresponding saturation in the hardness values at the edge of the disk so that, ultimately, there is a fairly homogeneous distribution of hardness across the disk. There have been numerous discussions on the significance of this saturation grain size [22, 23]. Clearly, the occurrence of a saturation in the grain size and a general homogeneity is

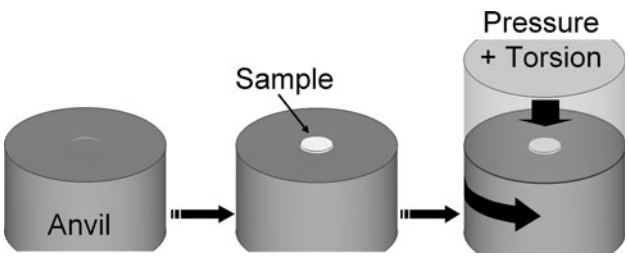

Fig. 1 Illustration of the principle of quasi-constrained high-pressure torsion

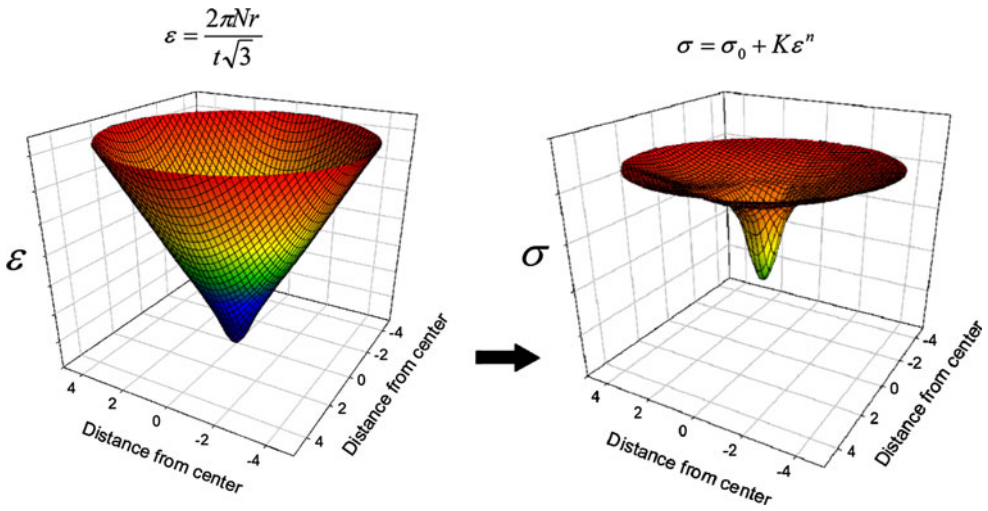

Fig. 2 Theoretical distribution of plastic strain ε and strength σ along the surface of a disk processed by HPT

not consistent with the theoretical prediction of plastic strain which predicts a region of very low strain at the center of the disk for any number of turns. It is, however, consistent with a model for HPT developed using strain gradient plasticity [24]. There are also additional differences such as variations in the distributions of microhardness with variations in the applied pressure [17–19] which are not predicted by the theory and variations in the distributions of hardness within samples in the through-thickness direction [25–28]. All of these results show that a more detailed analysis of plastic flow is required in order to provide a better explanation of the experimental results.

The use of FEM provides a valuable tool for describing and evaluating the plastic flow during HPT and it may also be used to evaluate the effect of some specific processing parameters. The earliest reports of HPT using FEM focused on unconstrained HPT where the disk was free to flow outwards during processing [29–31] and these analyses showed reductions in the thickness of the samples during processing and heterogeneous distributions of hydrostatic stresses. More recently, the focus has turned to quasi-constrained HPT where the sample is partially constrained within depressions on the lower and upper anvils [32–35] and this is consistent with the operating process generally used in most modern HPT facilities. From these analyses, it was demonstrated that material will flow outwards between the two anvils and this will also lead to a reduction in the sample thickness [32]. For the quasi-constrained conditions, the distributions of strain agree with the theoretical distribution if the reduction in sample thickness is included in the analysis and it was shown that the compressive stress state is larger at the center and decreases at the edge of the disk. The mean stresses also decrease with the material outflow and this effectively increases the sample area [32].

Calculations show that a significant temperature rise takes place during HPT processing and this is more pronounced in hard materials and/or during processing at faster rotation rates [33, 34]. Recently, it was shown, using 2D [35] and 3D simulations [36], that the distribution of strain varies also along the sample through-thickness, where the source of this heterogeneity was attributed to material behavior, friction, and the sample diameter-to-thickness ratio [35].

The use of finite element modeling

Simulations were performed using the FEM DEFORM-3D software, version 10.0 (Scientific Forming Technologies Corporation, Columbus, OH). The geometry of the anvils was arranged to simulate a quasi-constrained facility and the anvils were designed as cylindrical rigid bodies with diameters of 50 mm, thicknesses of 20 mm and with a shallow depression, 0.25 mm in depth and 10 mm in diameter, on the inner faces of each anvil. The lateral walls at the edge of the depressions had inclinations of 22° to the depression surface and a radius of curvature of 0.01 mm was considered in the corner edges of the depressions. A friction coefficient between 0.28 and 0.32 (Coulomb-type friction) was considered for the contact between the sample and the anvil in this region. The HPT sample was designed as a rigid-plastic disk element having a diameter of 10 mm and thickness of 0.8 mm. In order to investigate the effect of the sample thickness, some simulations used sample thicknesses of 1.8 and 3.8 mm and for these disks the anvil depression depths were increased to 0.6 and 1.5 mm, respectively.

During the simulation, an axial force in the range 78,600–314,200 N was applied to the top anvil where this

force range was selected to simulate theoretical pressures in the range from 1.0 to 4.0 GPa. The lower anvil was forced to rotate with a constant rotation rate of 1 rpm and without any movement in the axial direction. A sticking condition was imposed at the contacts between the disk surfaces and the bottoms of the anvil depressions. This condition was used to prevent any slippage between the sample and the anvil, and it is consistent with an earlier report showing an absence of slippage between the sample and the anvil at least for soft materials under sufficient pressure [37]. In practice, it should be noted that the bottoms of the depressions in HPT anvils are generally treated, for example, by nitriding, in order to attain a high roughness that prevents slippage. There is an opposite trend both at the lateral walls around the depression and outside of the depression on the anvil surface, in the outflow area, where there is good finishing with low roughness in order to prevent friction between the disk and the anvils. For the present simulations, the coulomb friction in these areas was represented by a friction coefficient of 0.3. The width of the outflow area was considered as 3 mm. As there are reports of different microhardness evolutions in samples processed under different pressures [17, 38], the Coulomb friction was considered because it is expected that the pressure plays a role in determining the contact friction between the anvil and the sample.

The workpiece was modeled as a rigid-plastic object in which the flow stress determines the beginning of plastic flow. A mesh with $\sim$60,000 elements was introduced in the workpiece with finer elements near the edge of the sample in order to provide a detailed analysis of localized plastic flow in the peripheral region. Preliminary simulations showed that the level of the flow stress plays only a minor role in the plastic flow during HPT and instead the major effect is due to the evolution of the flow stress as a function of strain. To incorporate this result, the effect of material behavior on plastic flow was examined using three different theoretical ideal materials which are labeled strain-hardening, perfect-plastic, and flow-softening. The behavior of the strain-hardening and perfect-plastic conditions were modeled using Hollomon-type equations of the form $\sigma = K\varepsilon^n$, where σ is the flow stress, K is a constant, ε is the effective plastic strain, and n is the strain-hardening coefficient. For the strain-hardening behavior, the model used a high value of $n = 0.3$ and $K = 500$ MPa. For the perfect-plastic behavior, the model used a low value of $n = 0.02$ and $K = 1{,}000$ MPa. The flow-softening behavior was modeled as a linear relationship between flow stress and the effective plastic strain of the form $\sigma = (1{,}000 - \varepsilon)$ MPa. These theoretical forms of material behavior were employed to provide qualitative information on the effect of hardening or softening within the workpiece during processing by HPT.

The results for the simulations

The simulations showed a continuous increase in the imposed plastic deformation to the sample where the extent of the deformation is proportional to the amount of rotation which depends on the time. Figure 3 shows the distribution of the effective stress on the top surface of a sample at different levels of rotation for a strain-hardening material tested under a pressure of 2.0 GPa. Separate distributions are illustrated after 1/12, 1/6, and 1/2 rotations with the flow stresses illustrated pictorially using the color key shown on the right. It is apparent that the effective stress distribution is not linear. Instead, it varies significantly near the center of the disk and the variation in stress is smaller near the edge. It is also apparent that the effective stress increases with increasing rotation.

The simulations showed that plastic deformation takes place in a near steady-state manner. In fact, the analysis demonstrated that the only variation in plastic flow during steady-state torsion is associated with the progressive outflow of material around the edge of the disk between the two anvils. This outflow or extrusion, often termed the flash, serves to reduce the sample thickness during the processing operation. As the deformation takes place in steady-state conditions, the instantaneous distribution of strain rate provides a good description of the plastic flow as the plastic deformation depends only on the amount of time for deformation. Accordingly, Figs. 4, 5, and 6 show the distributions of strain rate, on a similar scale, for different material conditions and using different fundamental processing parameters. All of these samples were cut in half along the central diameter in order to show the distributions of strain rate both on the longitudinal section and within the through-thickness.

In Fig. 4, the plastic flow is presented for simulations based on considerations of the three different types of material behavior using an applied pressure of 2.0 GPa. It is concluded that all simulations exhibit a continuous increase in the rate of plastic flow with increasing distance from the center of the disk. It is also observed that the distribution of the rate of plastic flow is almost constant in the through-thickness direction except only for very small regions near the edges of the disks where small variations are observed. It is also apparent that the variation in the rate of plastic flow within the sample thickness in the region near the edge of the disk is more pronounced in the sample with perfect-plastic behavior compared to the sample with strain-hardening behavior. It is worth noting that, in practice, the distribution of strain rate in strain-hardening materials evolves to the distribution observed in perfect-plastic materials at large number of rotations due to saturation in hardening capability.

Figure 5 shows the rate of plastic flow in simulations where the initial thicknesses of the sample were varied:

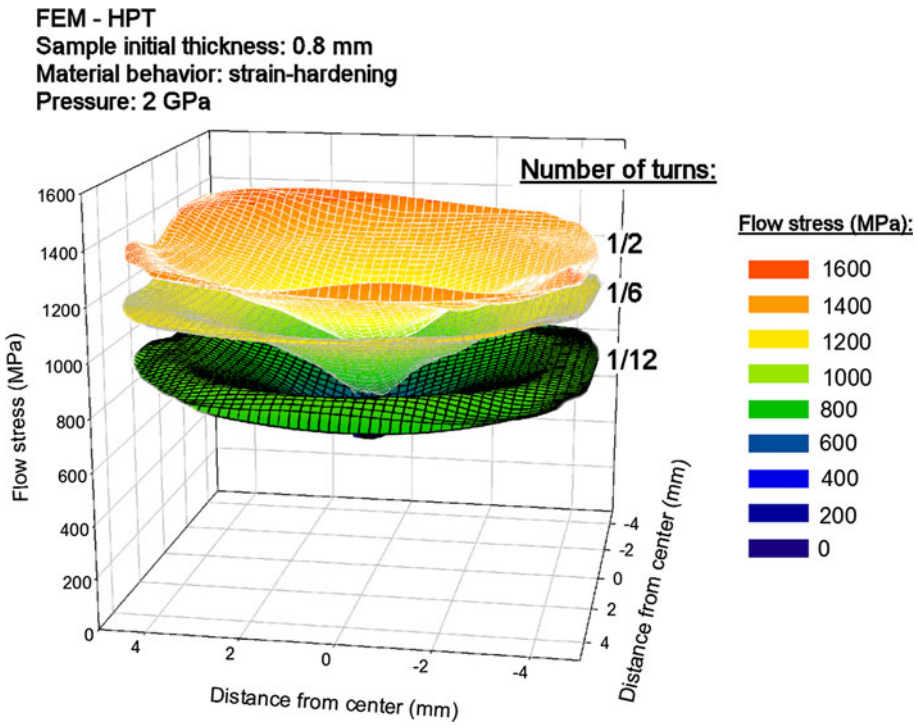

Fig. 3 Distribution of effective stress across the disk surface after processing a strain-hardening material for 1/12, 1/6, and 1/2 turn of HPT

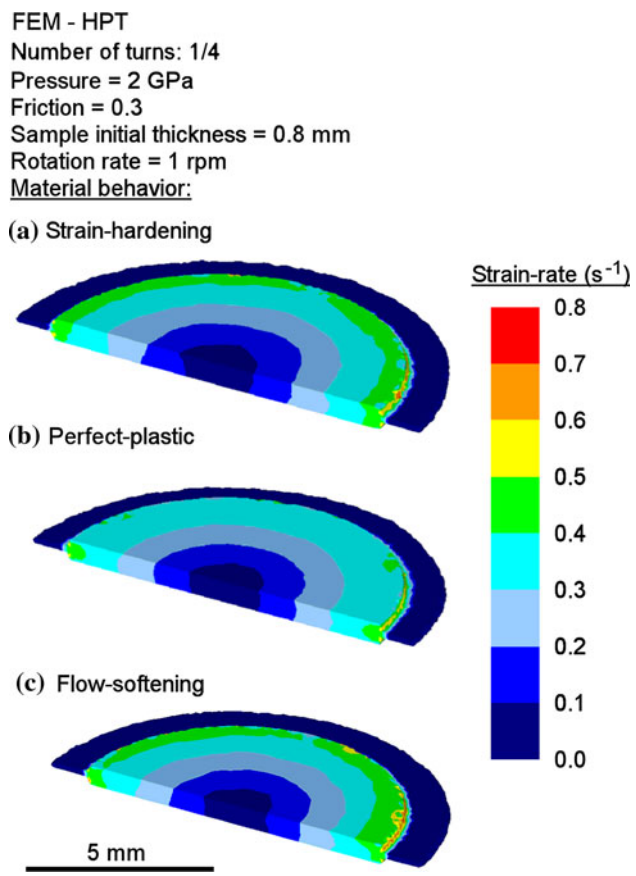

Fig. 4 Distribution of strain rate on the half-disk surfaces and along the disk longitudinal sections considering samples with **a** strain-hardening, **b** perfect-plastic, and **c** flow-softening behavior

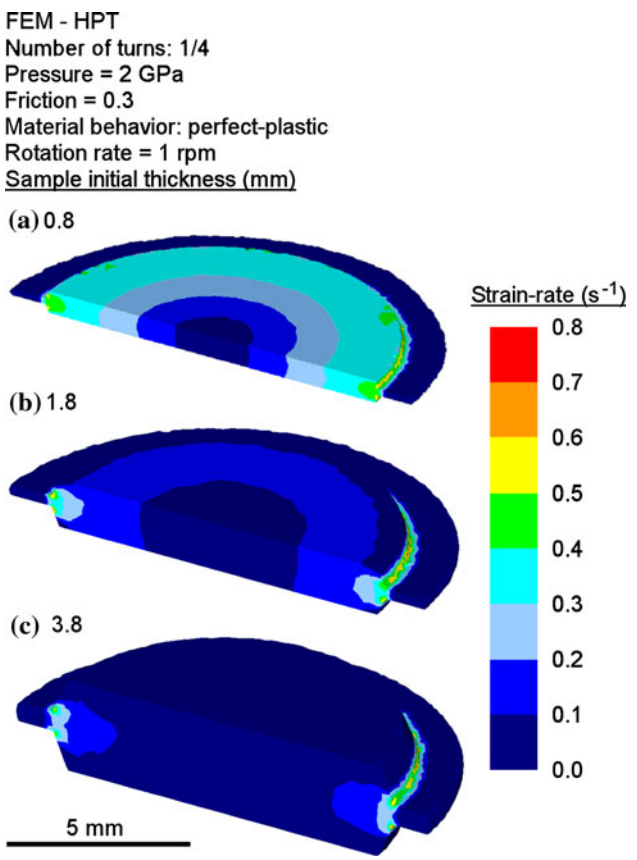

Fig. 5 Distribution of strain rate on the half-disk surfaces and along the disk longitudinal sections considering samples having initial thicknesses of **a** 0.8, **b** 1.8, and **c** 3.8 mm

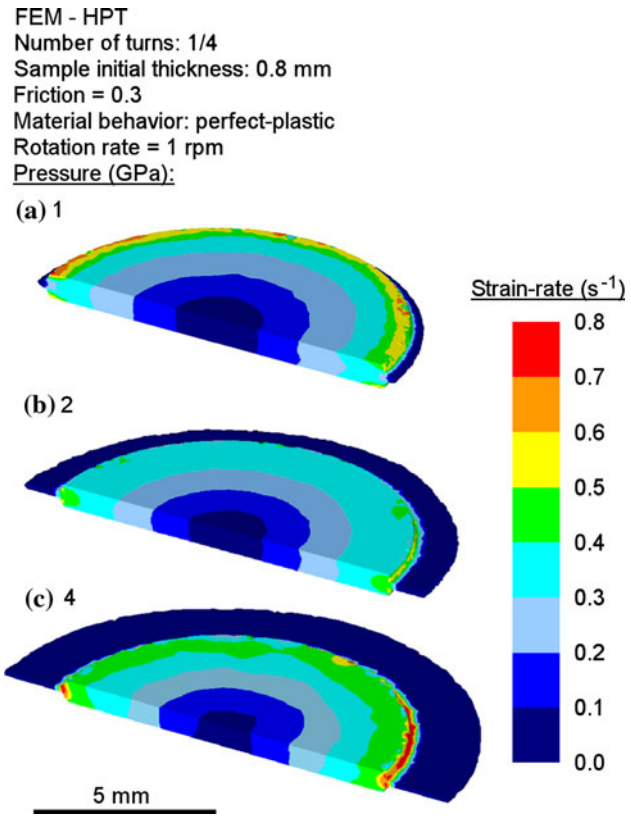

Fig. 6 Distribution of strain rate on the half-disk surfaces and along the disk longitudinal sections considering HPT processing with nominal pressures of **a** 1, **b** 2, and **c** 4 GPa

specifically, the sample thicknesses are (a) 0.8, (b) 1.8, and (c) 3.8 mm and the applied pressure remains at 2.0 GPa. These simulations show the strain rate is higher near the edge of the samples and around the mid-plane. It is also noted that the variation in the rate of plastic flow within the through-thickness direction is more pronounced in the samples having smaller diameter-to-thickness ratios.

The final set of illustrations in Fig. 6 shows the distribution of strain rate in samples processed under different nominal pressures of (a) 1, (b) 2, and (c) 4 GPa. It is readily apparent that, as anticipated, an increasing pressure increases the material outflow between the anvils, where this is characterized by a wider border for the samples. There is also a change in the flow pattern as the sample processed at the lowest pressure exhibits a concentration of plastic flow near the surface at the edge of the disk, whereas the sample processed at the highest pressure exhibits a concentration of plastic flow near the mid-plane.

The effect of the nominal pressure is also evident in the distributions of flow stresses along the top surfaces of the disks as shown in Fig. 7 for simulations involving the two pressures of 1 GPa (the mesh with black lines) and 4 GPa (the mesh with white lines). A continuous increase in flow stress with increasing distance from the center is observed in the sample processed at the lower nominal pressure, whereas there is a small region with decreasing flow stress near the edge of the disk after processing at the higher nominal pressure.

The effect of friction is addressed in Fig. 8 where simulations are shown for samples processed by HPT considering different values for the friction coefficients between the top and bottom anvils. To provide a direct comparison, simulations are also shown for similar friction coefficients in Fig. 8a, c for pressures of 1 and 4 GPa, respectively. The simulations consider a low level of nominal pressure for the top surface and a high pressure for the bottom surface. The results from these calculations demonstrate that the use of distinct friction coefficients leads to a concentration of plastic flow on one side of the disk. Specifically, the concentration of plastic flow occurs on the side having the lower friction coefficient. Furthermore, this effect is observed at both levels of nominal pressure but the concentration is more obvious at the higher pressure in Fig. 4d.

Discussion

The present results provide a broad understanding of the distribution of plastic deformation in samples processed by HPT. The influences of different processing parameters are evaluated and it is possible to correlate the findings both to the theory of plastic deformation and to publish experimental results. The main points of agreement and disagreement are examined in the following sections.

Agreement with theory

These results agree with the theoretical prediction incorporated in Eq. 1 of increasing plastic deformation with increasing distance from the center of the disk. A nearly linear increase in strain rate with increasing distance from the disk center is observed in Fig. 4 for all material behavior. The increase in plastic deformation with distance to the center and with the number of rotations is expected to lead to an increase in strength both with increasing distance to the center and with increasing rotation. This effect is confirmed in Fig. 3 for a strain-hardening material.

Disagreement with theory

The present results disagree with the theory of plastic flow on some points. First, heterogeneities in the distributions of plastic deformation are observed along the sample thickness and this is more obvious near the edges of the disks and in thicker samples. This heterogeneity is not predicted by the theory. Also, the theory predicts no influence of hydrostatic pressure on the plastic flow but the present

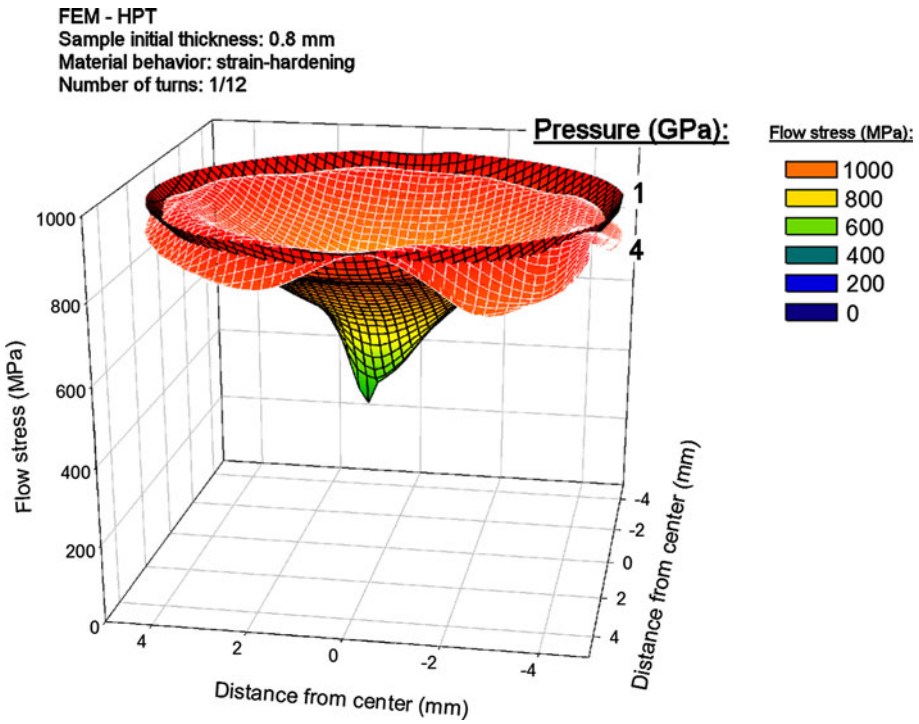

Fig. 7 Effective stress plotted as a function of the distance from the center of the sample considering HPT processing with nominal pressures of 1 GPa (*black lines*) and 4 GPa (*white lines*)

calculations show this parameter affects the plastic flow near the lateral walls of the depressions in the anvils.

Agreement with experiments

Although the present results disagree with the theory of plastic flow in some respects, they generally agree and confirm the experimental results available in the literature. The increase in strength with increasing distance to the disk center is in agreement with many observations of increasing hardness with increasing distance to the centers of disks processed by HPT [15–21]. In fact, the shapes of the curves of the distributions of strength in Fig. 3 are analogous to the shapes of the curves of the distributions of hardness available in the literature [21].

Moreover, heterogeneities of plastic flow along the sample thickness were reported in experiments and this trend is confirmed by the present calculations. For example, the development of heterogeneous plastic flow during HPT was first observed in a thick aluminum sample [25] and later it was shown that regions of low deformation are formed at the edges of disks near the surfaces [26]. This leads to higher deformation around the mid-plane of the disks at the expense of deformation near the surface. Thus, higher microhardness was observed near the mid-plane and it was found that the difference in microhardness between the surface and the mid-plane regions increase with increasing sample thickness [26]. Again, this trend is confirmed by the present results. A recent report described the formation of a dead metal zone in this region [36] and the heterogeneities were attributed to the inclination of the lateral wall in HPT [26] and high friction between the sample and this lateral wall [36]. In fact, it was shown that the heterogeneity of plastic deformation decreased when the inclination of the lateral wall was increased [26].

The present results confirm the influence of the friction at the lateral wall on the overall heterogeneity and the results show this is influenced by the nominal pressure imposed during HPT. At low pressures, a low friction develops between the sample and the anvil and an opposite trend is observed. A concentration of plastic flow is observed near the surface at the expense of the deformation near the mid-plane of the sample. This is similar to results reported in 2D simulations when the friction between the sample and the lateral wall was reduced [35]. In addition, other reports [15, 17, 18] have shown that the nominal pressure affects the distribution of microhardness along the disk surface and this effect is not predicted by the theory. The present simulations confirm there are variations in the distributions of the effective stress with variations in the nominal pressure and this would become evident in microhardness testing. These variations are explained by changes in the friction coefficient between the sample and the anvil which controls the plastic flow during HPT at least near the edge of the disk.

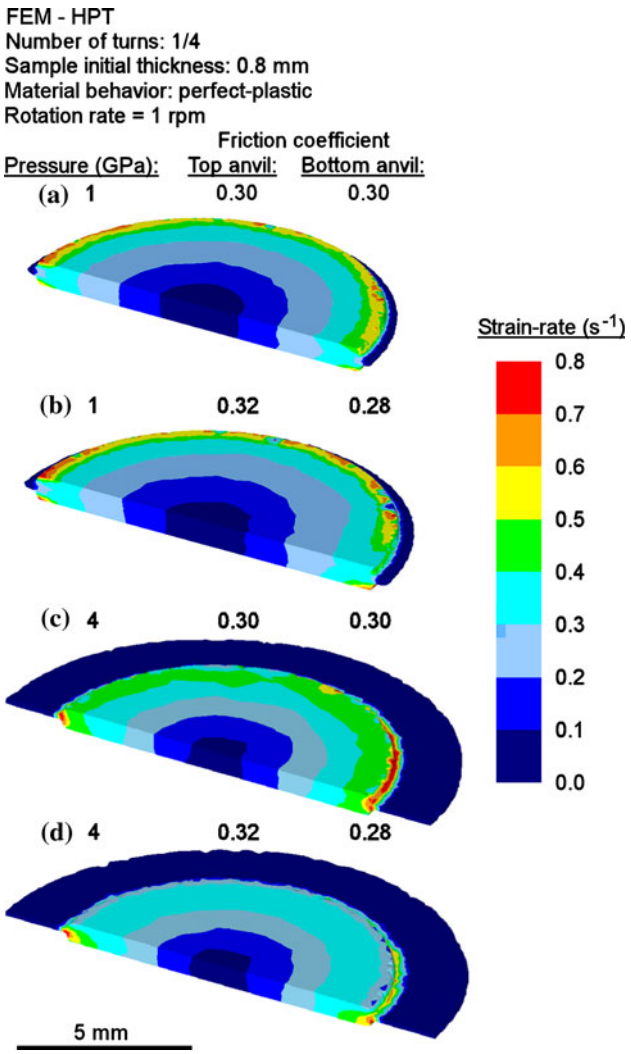

Fig. 8 Distribution of strain rate on the half-disk surfaces and along the disk longitudinal sections considering HPT processing with nominal pressures of **a**, **b** 1 GPa and **c**, **d** 4 GPa: the contact friction between the sample and the anvil top and bottom walls is considered similar in **a**, **c** and different in **b**, **d**

Summary and conclusions

1. Three-dimensional FEM was used to simulate plastic flow during quasi-constrained HPT. Simulations were conducted to examine the effect of material behavior, the sample aspect ratio, the nominal pressure, and the friction between the sample and the depressions on the anvil surfaces.
2. The results confirm the theoretical predictions and show increases in strength with increasing distance to the centers of the disks and with increasing rotation in strain-hardening materials.
3. The results contradict the theoretical prediction and show the presence of heterogeneous plastic flow along the sample thickness. This tendency is more obvious near the edge of the disks and is attributed to the friction between the sample and the lateral walls of the depressions on the anvil surfaces.
4. The nominal pressure during HPT plays a major role in the contact friction between sample and anvil, and this affects the plastic flow and the distribution of strength along the sample surface. These observations are in agreement with experimental observations reported in the literature.

Acknowledgements This work was supported in part by the Brazilian Research Council (CNPq) and in part by the European Research Council under ERC Grant Agreement No. 267464-SPDMETALS. R.B. Figueiredo also acknowledges support from PPGEM (Programa de Pós-Graduação em Engenharia Metalúrgica, de Materiais e de Minas da Universidade Federal de Minas Gerais).

References

1. Valiev RZ, Islamgaliev RK, Alexandrov IV (2000) Prog Mater Sci 45:103
2. Valiev RZ, Langdon TG (2006) Prog Mater Sci 51:881
3. Zhilyaev AP, Langdon TG (2008) Prog Mater Sci 53:893
4. Iwahashi Y, Wang J, Horita Z, Nemoto M, Langdon TG (1996) Scripta Mater 35:143
5. Nakashima K, Horita Z, Nemoto M, Langdon TG (1998) Acta Mater 46:1589
6. Iwahashi Y, Horita Z, Nemoto M, Langdon TG (1998) Acta Mater 46:3317
7. Yamashita A, Yamaguchi D, Horita Z, Langdon TG (2000) Mater Sci Eng A287:100
8. Prell M, Xu C, Langdon TG (2008) Mater Sci Eng A480:449
9. Alhajeri SN, Gao N, Langdon TG (2011) Mater Sci Eng A528:3833
10. Semiatin SL, DeLo DP, Shell EP (2000) Acta Mater 48:1841
11. Kim HS, Seo MH, Hong SI (2000) Mater Sci Eng A291:86
12. Li S, Bourke MAM, Beyerlein IJ, Alexander DJ, Clausen B (2004) Mater Sci Eng A382:217
13. Figueiredo RB, Cetlin PR, Langdon TG (2007) Acta Mater 55:4769
14. Valiev RZ, YuV Ivanisenko, Rauch EF, Baudelet B (1996) Acta Mater 44:4705
15. Zhilyaev AP, Nurislamova GV, Kim B-K, Baró MD, Szpunar JA, Langdon TG (2003) Acta Mater 51:753
16. Vorhauer A, Pippan R (2004) Scripta Mater 51:921
17. Xu C, Horita Z, Langdon TG (2008) Acta Mater 56:5168
18. Xu C, Langdon TG (2009) Mater Sci Eng A503:71
19. Loucif A, Figueiredo RB, Baudin T, Brisset F, Langdon TG (2010) Mater Sci Eng A527:4864
20. Wongsa-Ngam J, Kawasaki M, Zhao Y, Langdon TG (2011) Mater Sci Eng A528:7715
21. Kawasaki M, Alhajeri SN, Xu C, Langdon TG (2011) Mater Sci Eng A529:345
22. Pippan R, Wetscher F, Hafok M, Vorhauer A, Sabirov I (2006) Adv Eng Mater 8:1046
23. Pippan R, Scheriau S, Taylor A, Hafok M, Hohenwarter A, Bachmaier A (2010) Ann Rev Mater Res 40:319
24. Estrin Y, Molotnikov A, Davies CHJ, Lapovok R (2008) J Mech Phys Solids 56:1186
25. Sakai G, Nakamura K, Horita Z, Langdon TG (2005) Mater Sci Eng A406:268

26. Hohenwarter A, Bachmaier A, Gludovatz B, Scheriau S, Pippan R (2009) Int J Mater Res 100:12
27. Figueiredo RB, Langdon TG (2011) Mater Sci Eng A528:4500
28. Figueiredo RB, Aguilar MTP, Cetlin PR, Langdon TG (2011) Metall Mater Trans 42A:3013
29. Kim HS (2001) J Mater Proc Technol 113:617
30. Kim HS, Hong SI, Lee YS, Dubravina AA, Alexandrov IV (2003) J Mater Proc Technol 142:334
31. Yoon SC, Horita Z, Kim HS (2008) J Mater Proc Technol 201:32
32. Figueiredo RB, Cetlin PR, Langdon TG (2011) Mater Sci Eng A528:8198
33. Edalati K, Miresmaeili R, Horita Z, Kanayama H, Pippan R (2011) Mater Sci Eng A528:7301
34. Figueiredo RB, Pereira PHR, Aguilar MTP, Cetlin PR, Langdon TG (2012) Acta Mater 60:3190
35. Figueiredo RB, Aguilar MTP, Cetlin PR, Langdon TG (2012) J Mater Sci 47:4807
36. Lee DJ, Yoon EY, Park LJ, Kim HS (2012) Scripta Mater 67:384
37. Edalati K, Horita Z, Langdon TG (2009) Scripta Mater 60:9
38. Kawasaki M, Ahn B, Langdon TG (2010) Acta Mater 58:919